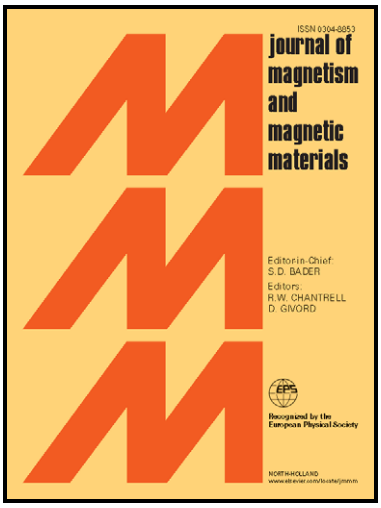

Hysteresis Magnetoresistance and Micromagnetic Modeling of Ni Microbelts

Zhi-Min Liao, Yi Lu, Hong-Zhou Zhang, Da-Peng Yu

PII: S0304-8853(10)00082-X
DOI: doi:10.1016/j.jmmm.2010.02.016
Reference: MAGMA 56103

To appear in: *Journal of Magnetism and Magnetic Materials*

Received date: 14 October 2009
Revised date: 7 February 2010
Accepted date: 9 February 2010

Cite this article as: Zhi-Min Liao, Yi Lu, Hong-Zhou Zhang and Da-Peng Yu, Hysteresis Magnetoresistance and Micromagnetic Modeling of Ni Microbelts, *Journal of Magnetism and Magnetic Materials*, doi:10.1016/j.jmmm.2010.02.016

Hysteresis Magnetoresistance and Micromagnetic Modeling of Ni Microbelts

Zhi-Min Liao[a,*], *Yi Lu*[b], *Hong-Zhou Zhang*[c], *Da-Peng Yu*[a,*]

[a]*State Key Laboratory for Mesoscopic Physics, Department of Physics, Peking University, Beijing 100871, P. R. China*

[b]*Yuanpei College, Peking University, Beijing 100871, P. R. China*

[c]*School of Physics and Centre for Research on Adaptive Nanostructures and Nanodevices (CRANN), Trinity College, Dublin 2, Ireland.*

Abstract

Magnetization reversal process in a single nickel microbelt is investigated by measuring magnetoresistance (MR). A hysteresis MR curve is observed, which consists of a reversible bell-shaped curve under high magnetic field and an irreversible discontinuity under low magnetic field. A micromagnetic simulation is performed for understanding the underlying physics behind the MR curve. The hysteresis is ascribed to the competition of exchange energy and Zeeman energy, and the irreversible discontinuity is attributed to the formation of domain walls and vortices.

Keywords: Nanostructures; Nickel; Magnetoresistance; Magnetization reversal; Magnetic vortices.

*Corresponding authors.

E-mail addresses: liaozm@pku.edu.cn (Z.M. Liao), yudp@pku.edu.cn (D.P. Yu)

1. Introduction

Magnetization states and reversal mechanisms in magnetic nanostructures are of great interests during the past decades because of the emergence of novel size-dependent effects and the potential applications in magnetic nonvolatile memory devices [1-5]. Several mechanisms have been proposed so far for magnetization reversal in ferromagnetic nanostructures: coherent rotation [6-7], curling [8-9], buckling [10-11], domain wall motion [12-13] etc. The magnetization reversal is dependent on the geometric parameters and the intrinsic magnetic properties of the ferromagnetic nanostructures. In order to explain the magnetization reversal, the process of nucleation and propagation of magnetic vortices have received special attention [14-16]. In recent years, anisotropic magnetoresistance (AMR) measurement has been attempted to develop a better understanding of the magnetization reversal in different nanostructures [17-20]. The AMR reflects the dependence of the electric resistivity with the angle between the directions of magnetization and current. It provides a highly sensitive probe to small changes in magnetization state. Abrupt jumps in the magnetoresistance (MR) curve in low magnetic fields were previously reported [20-24]. The correlation between the MR jumps and the magnetization variations induced by external magnetic field was also studied [24]. However, the detailed processes of magnetization evolution are usually different for the specimens with different shapes. Therefore, it is essential to investigate the process of magnetization evolution for better understanding of the magnetic properties of Ni nano/micro-structures.

In this work, we study the magnetization states in Ni microstructures through both experiments and numerical simulations. A jump of the MR curve was observed and the jumping process persisted ~250 Oe. The slowly varying jump reveals the reversal modes occurring in the magnetization process, especially the transition between different magnetization states. In addition, a hysteresis MR curve was also observed and discussed.

2. Experiments

The microstructure patterns were created by electron beam lithography on a SiO_2 substrate. Ni film with thickness of 20 nm was then deposited by electron beam evaporation on the patterned sample. To prevent oxidation, a 2-nm thick Au thin layer was deposited on top of the Ni layer. The scanning electron microscopy (SEM) image of a typical sample is presented in Fig. 1. The length, width, and thickness of the Ni microbelt is 6 μm, 1.3 μm, 20 nm, respectively and it was connected to two square pads. The square pads are 150×150 μm^2 in size. Current was injected into the center of the pads.

A constant dc current of 1 μA through the nickel microbelt was sustained by a Keithley 6221 Current Source. Longitudinal voltage was measured by a Keithley 2182A Nanovoltmeter. The sample was placed in an Oxford He cryostat system to maintain a constant temperature of 3.3 K during the whole experiment. An external magnetic field was applied perpendicularly to the sample plane by an Oxford VTI system. With a perpendicular external field, the effect of the magnetic field on the in-plane rotation of magnetic moments was investigated.

3. Results and discussion

Figure 2 shows the longitudinal MR data obtained in the experiment. A reversible bell-shaped curve under high magnetic field was observed. Under low magnetic fields, a hysteresis behavior can be seen clearly in the enlarged MR curve, as shown in Fig. 2b. As the magnetic field decreases from 5 kOe to -5 kOe (the red curve in Fig. 2), the resistance first increases, and then decreases after reaching a maximum at ~0.5 kOe, and a jump starts at -0.4 kOe and finisher at -0.64 kOe. Similar phenomenon is also found as the magnetic field sweeps from -5 kOe to 5 kOe (the black curve in Fig. 2).

To understand the magnetization reversal process, a micromagnetic simulation was carried out using OOMMF [25]. Magnetization state was calculated by solving the Landau–Lifshitz–Gilbert (LLG) equation for a model Ni microbelt. The

dimensions of the model structure are defined by the real structure measured. The LLG equation is given by

$$\frac{d\mathbf{m}}{dt} = -\gamma_0 \mathbf{m} \times \mathbf{H}_{\mathbf{eff}} + \alpha \mathbf{m} \times \frac{d\mathbf{m}}{dt}, \textbf{ (1)}$$

where γ_0 is the gyromagnetic ratio, $\mathbf{m} = \frac{\mathbf{M}}{M_s}$ is the normalized magnetization, and $\mathbf{H}_{\mathbf{eff}}$ is the effective magnetic field. The saturation magnetization was set to a typical value of $M_s = 4.9 \times 10^5 A/m$ in this calculation, and the Gilbert damping constant α was assumed to be 0.04 [26]. A coupling constant of $A = 9.0 \times 10^{-12} J/m$ was used for calculating the exchange energy. Then the MR curve was reproduced by the relation given by

$$\rho(H) = \rho_{\perp} + (\rho_{//} - \rho_{\perp}) \cos^2 \theta, \textbf{ (2)}$$

where $\rho_{\perp}$ and $\rho_{//}$ are the resistivities when the magnetization direction is perpendicular and parallel to the direction of the electrical current, respectively [27]. θ is the angle between the magnetization and the current direction. The projection of the total magnetization **M** on the microbelt axis can be expressed as $\mathbf{M_x} = \mathbf{M} \cos\theta$, and the normalized magnetization is $\mathbf{m_x} = \cos\theta$. Then Eq. 2 can be rewritten as

$$\rho(H) = \rho_{\perp} + (\rho_{//} - \rho_{\perp}) m_x^2. \textbf{ (3)}$$

Considering the inhomogeneous of the magnetization, we assume that the microbelt was divided into cells with a length of 10 nm, which is close to the exchange length of ~7.7 nm calculated by $\sqrt{2A/\mu_0 M_s^2}$. The resistance of each cell was calculated using Eq. 3. The equivalent resistance of the microbelt was then computed since the cells formed a electrical network [28]. The calculated MR curve is presented in Fig. 3. The bell shaped MR curve obtained by the simulation resembles the experimental data plotted in Fig. 2. A sudden jump of the MR was also evident from the simulated curve. However, the simulations do not quantitatively fit the experimental results. The micromagnetic simulations may be sensitive to the parameters, such as Ms values, anisotropy constants, and cell size. We have checked different values of the parameters for the simulations, but no obvious differences compared to Fig. 3 were obtained. The difference between the experimental and

calculated MR curves may be attributed to the edge roughness of the Ni microbelt and the magnetic contact pads. The non-ideal symmetries introduced by the edge roughness and the pads can have a huge impact in the nucleation process of magnetic vortices [14].

Although it is difficult to quantitatively explain the MR curves, the experimental results can be qualitatively interpreted by the magnetic states obtained from simulations. A detailed configuration of the magnetization reversal process for the field applied perpendicular to the sample plane is highly desired. At initial state, a field of 5 kOe is applied perpendicularly to the microbelt plane. Such magnetic field saturates the magnetization along the positive z-direction, as shown in Fig.4a. The magnetic moments tend to rotate toward the microbelt plane with the decrease of the magnetic field (see in Fig. 4b). Consequently, the M_x component increases and so does the magnetoresistance according to Eq. 3. As the magnetic field further decreases, magnetic vortices appear (see Fig. 4c). The magnetic vortices do not contribute to the in-plane magnetization and the M_x decreases, which may be the origin of the decrease of MR when the magnetic field approached zero.

The occurrence of magnetic vortices at low magnetic fields can be explained as follows. The atomic dipoles tend to align in parallel in the microbelt plane and form a spontaneous magnetization state to lower the exchange energy. On the other hand, the interaction of magnetic moments and the lattice results in alignment of individual moments along a preferential lattice direction. The atomic dipoles and the easy magnetization axis have different directions, and the competition of the dipolar interaction and the magnetocrystalline anisotropy leads to a wave like configuration of the magnetic moments. In addition, vortices always emerge at the ends of the microbelt. It is because a close-up magnetic flux ends up in a considerable reduction of the energy of demagnetizing field by avoiding the creation of poles at the surface.

According to the simulation, the magnetization divided into several domains separated by domain walls at zero field, as presented in Fig. 4c. As seen in Fig. 4d, the in-plane magnetization decreases with increasing the magnitude of the magnetic field

of negative polarity, which results in the decrease of MR. As the magnitude of the magnetic field of negative polarity further increases, the vortices at the two ends move to the center of the microbelt and produce another two vortices, which can be seen in Fig. 4e. Once the magnetic field exceeds the switching field (~ -0.4 kOe), adjacent domains merge into a larger domain and the magnetization along the microbelt axis increases. Therefore the magnetoresistance increases abruptly. Partial reversal of z-axis magnetization takes place when the magnetic field is lager than the switching field. The jump of the MR curve terminates when all the moments are reversed. The difference of switching field in Fig. 2 and Fig. 3 may result from the defects in the specimen and the choice of damping coefficient used for simulation. Neglecting the MR of the two rectangle pads might also cause the decrease in switching field.

To find more clues about the actual magnetization configurations at low fields, we performed a simulation where the field was applied with an incident angle of 15 degree. It could break the symmetry of the problem and results in the formation of more defined structures at low fields. Figure 5 shows the magnetization of the microbelt under different fields as denoted with 15 degree incident angle. It is found that vortices appear under low fields. When the applied field exceeds the switching field about 0.5 kOe, vortices merge into a larger domain and the magnetization projected on *x* axis increases. With the continuously increasing field, M_z increases and thus M_x decreases. When the field sweeps downwards, the magnetization various exactly the opposite with the upwards one except that the vortices disappear under low fields and a parallel magnetization occurs instead. This is because that the parallel alignment of the magnetic moments reduces the exchange energy and results in a smaller total energy compared to the initial random orientation. Therefore, the additional simulation confirms the formation of domains or vortex structures at low fields.

The magnetic contact pads which are not included in the simulation could affect the nucleation process. The rectangular pads could develop magnetic structures at low fields, which might modify the overall MR response. The pinning and depinning of

the domain walls at the interface of the microbelt and the pads might also lead to the variation of MR. Therefore, it may be possible to get the quantitative agreement between the simulated and measured MR curves by taking the complex sample configuration into account.

4. Conclusion

The magnetization reversal and MR hysteresis of a Ni microbelt were investigated experimentally and numerically. For external magnetic field applied perpendicular to the microbelt plane, the MR curve exhibits a discontinuity corresponding to magnetization reversal. The process of the discontinuity persists 250 Oe and it is ascribed to the formation of several domains and vortices in the microbelt plane. The incoherent magnetization state is confirmed by a micromagnetic calculation using OOMMF package. The hysteresis MR behavior in such a simple structure may provide an alternative method of logic and memory operations and promise a smaller scale of magnetic-recording devices.

Acknowledgment

This work was supported by NSFC (No. 10804002), MOST (Nos. 2007CB936202, 2009CB623703), the National Found for Fostering Talents of Basic Science (Grant No. J0630311, NFFTBS), and the Research Fund for the Doctoral Program of Higher Education (RFDP), Ministry of Education, P. R. China.

References

[1] D. A. Allwood, G. Xiong, C. C. Faulkner, D. Atkinson, D. Petit, and R. P. Cowburn, Science **309** (2005) 1688.

[2] C. Chappert, A. Fert, and F. N. Van Dau, Nat. Mater. **6** (2007) 813.

[3] S. S. P. Parkin, M. Hayashi, and L. Thomas, Science **320** (2008) 190.

[4] S. Tehrani, E. Chen, M. Durlam, M. DeHerrera, J. M. Slaughter, J. Shi, and G. Kerszykowski, J. Appl. Phys. **85** (1999) 5822.

[5] Z. M. Liao, Y. D. Li, J. Xu, J. M. Zhang, K. Xia, and D. P. Yu, Nano Lett. **6** (2006) 1087.

[6] Y. Jaccard, P. Guittienne, D. Kelly, J. E. Wegrowe, and J. P. Ansermet, Phys. Rev. B **62** (2000) 1141.

[7] H. Schmidt, J. Appl. Phys. **93** (2003) 2107.

[8] A. Aharoni, J. Appl. Phys. **82** (1997) 1281.

[9] Y. Ishii, J. Appl. Phys. **70** (1991) 3765.

[10] A. B. Oliveira, S. M. Rezende, and A. Azevedo, Phys. Rev. B **78** (2008) 024423.

[11] N. A. Usov, C. R. Chang, and Z. H. Wei, Phys. Rev. B **66** (2002) 184431.

[12] R. D. McMichael and M. J. Donahue, IEEE T. Magn. **33** (1997) 4167.

[13] K. W. Moon, J. C. Lee, M. H. Jung, K. H. Shin, and S. B. Choe, IEEE T. Magn. **45** (2009) 2485.

[14] P. Vavassori, N. Zaluzec, V. Metlushko, V. Novosad, B. Ilic, and M. Grimsditch, Phys. Rev. B **69** (2004) 214404.

[15] W. Casey Uhlig and J. Shi, Appl. Phys. Lett. **84** (2004) 759.

[16] B. Hong, T. J. Hayward, C. H. W. Barnes, and J.-R. Jeong, IEEE T. Magn. **45** (2009) 2511.

[17] S. Pignard, G. Goglio, A. Radulescu, L. Piraux, S. Dubois, A. Declemy, and J. L. Duvail, J. Appl. Phys. **87** (2000) 824.

[18] W. Wernsdorfer, B. Doudin, D. Mailly, K. Hasselbach, A. Benoit, J. Meier, J. P. Ansermet, and B. Barbara, Phys. Rev. Lett. **77** (1996) 1873.

[19] Y. Rheem, B. Y. Yoo, W. P. Beyermann, and N. V. Myung, Nanotechnology **18** (2007) 015202.

[20] T. Y. Chung and S. Y. Hsu, J. Appl. Phys. **103** (2008) 07C506.

[21] J. E. Wegrowe, D. Kelly, A. Franck, S. E. Gilbert, and J. P. Ansermet, Phys. Rev. Lett. **82** (1999) 3681.

[22] Y. Rheem, B. Y. Yoo, W. P. Beyermann, and N. V. Myung, Nanotechnology **18** (2007) 125204.

[23] A. N. Abdi and J. P. Bucher, Appl. Phys. Lett. **82** (2003) 430.

[24] P. Vavassori, M. Grimsditch, V. Metlushko, N. Zaluzec, and B. Ilic, Appl. Phys. Lett. **86** (2005) 072507.

[25] M. J. Donahue and D. G. Porter, in *Interagency Report NISTIR 6376* (National Institute of Standards and Technolog, Gaithersburg, MD, 1999).

[26] A. Barman, S. Wang, J. Maas, A. R. Hawkins, S. Kwon, J. Bokor, A. Liddle, and H. Schmidt, Appl. Phys. Lett. **90** (2007) 202504.

[27] R. C. O'Handley, in *Modern Magnetic Materials: Principles and Applications* (Wiley, 1999).

[28] R. A. Silva, T. S. Machado, G. Cernicchiaro, A. P. Guimaraes, and L. C. Sampaio, Phys. Rev. B **79** (2009) 134434.

Figure Captions

Fig. 1 SEM image of a ferromagnetic Ni microbelt having length of 6 μm, width of 1.3 μm, and thickness of 20 nm.

Fig. 2 (a) Longitudinal MR as a function of the magnetic field perpendicularly to the sample plane. Up-field sweep and down-sweep curves are colored in black and red respectively. (b) Zoom of the magnetoresistance under low magnetic fields.

Fig. 3 MR curve obtained by micromagnetic calculation using OOMMF method.

Fig. 4 Magnetization evolution in the microbelt plane as the magnetic field sweeping from positive high value to negative high value. The presented magnetic states are obtained at (a) high positive magnetic field, (b) intermediate positive field, (c) zero magnetic field, (d) negative intermediate field and (e) negative switching field.

Fig. 5 Simulated magnetization configurations with the applied field as denoted with an incident angle of 15 degree.

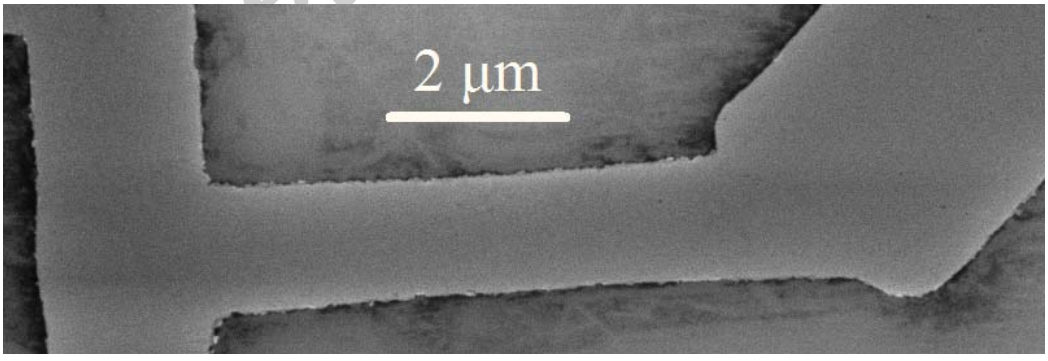

Fig. 1. SEM image of a ferromagnetic Ni microbelt having length of 6 μm, width of 1.3 μm, and thickness of 20 nm.

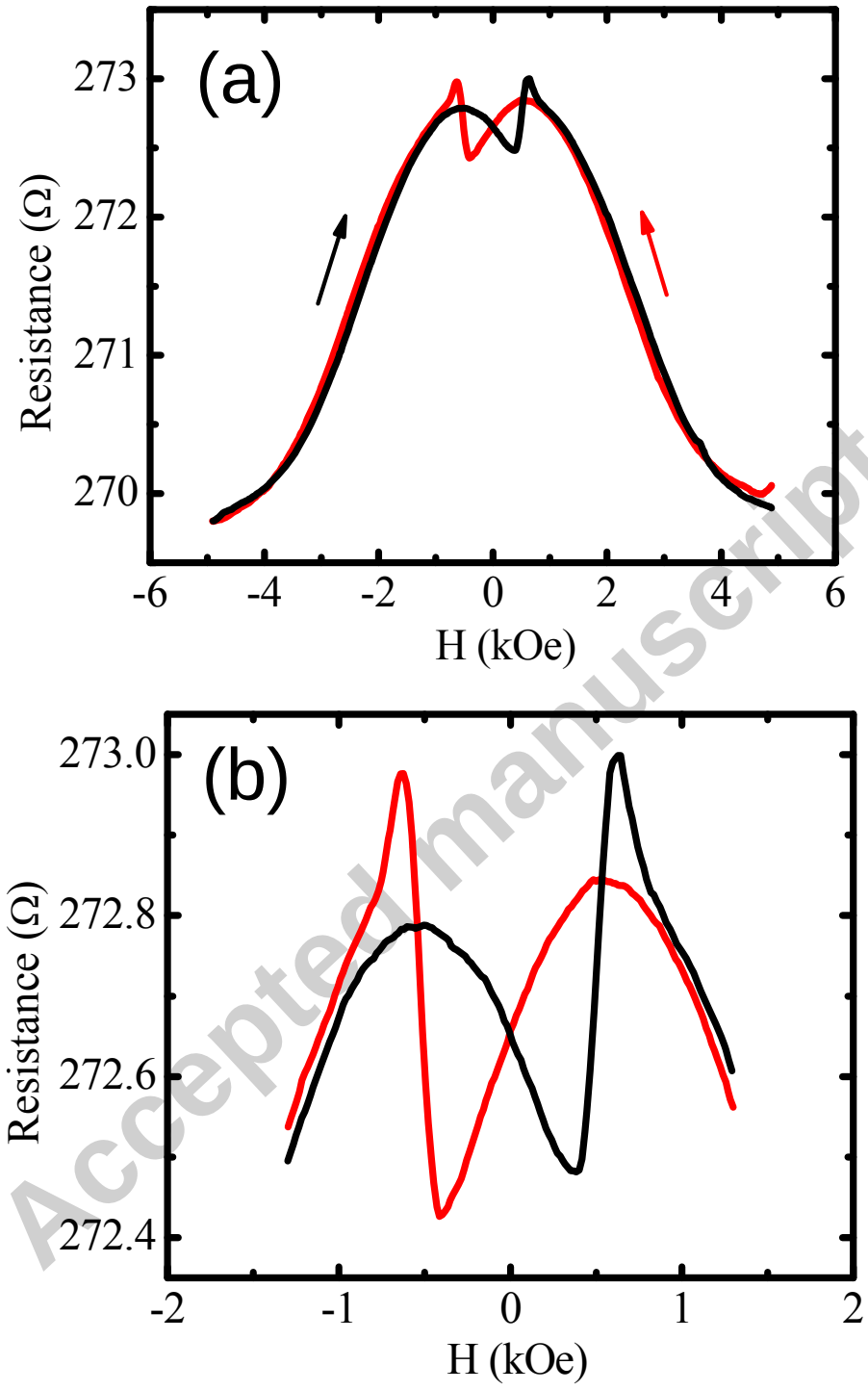

Fig. 2. (a) Longitudinal MR as a function of the magnetic field perpendicularly to the sample plane. Up-field sweep and down-sweep curves are colored in black and red respectively. (b) Zoom of the magnetoresistance under low magnetic fields.

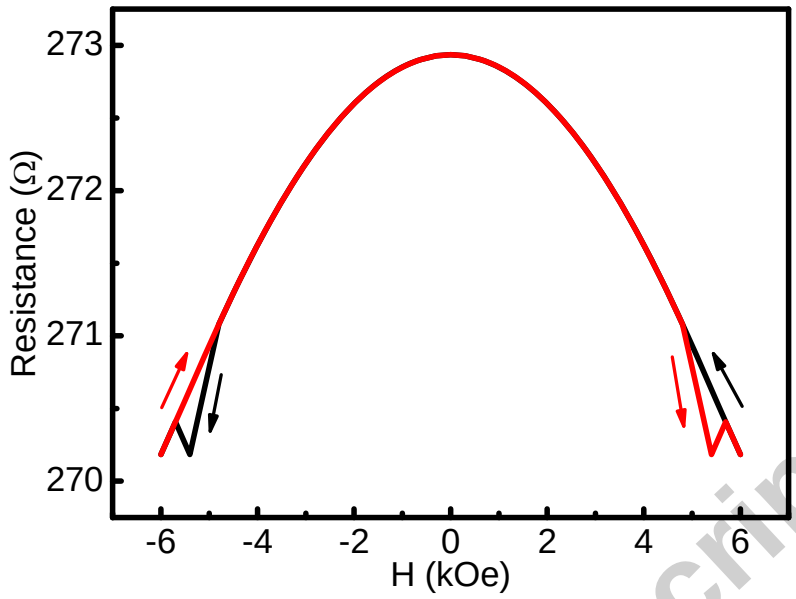

Fig. 3. MR curve obtained by micromagnetic calculation using OOMMF method.

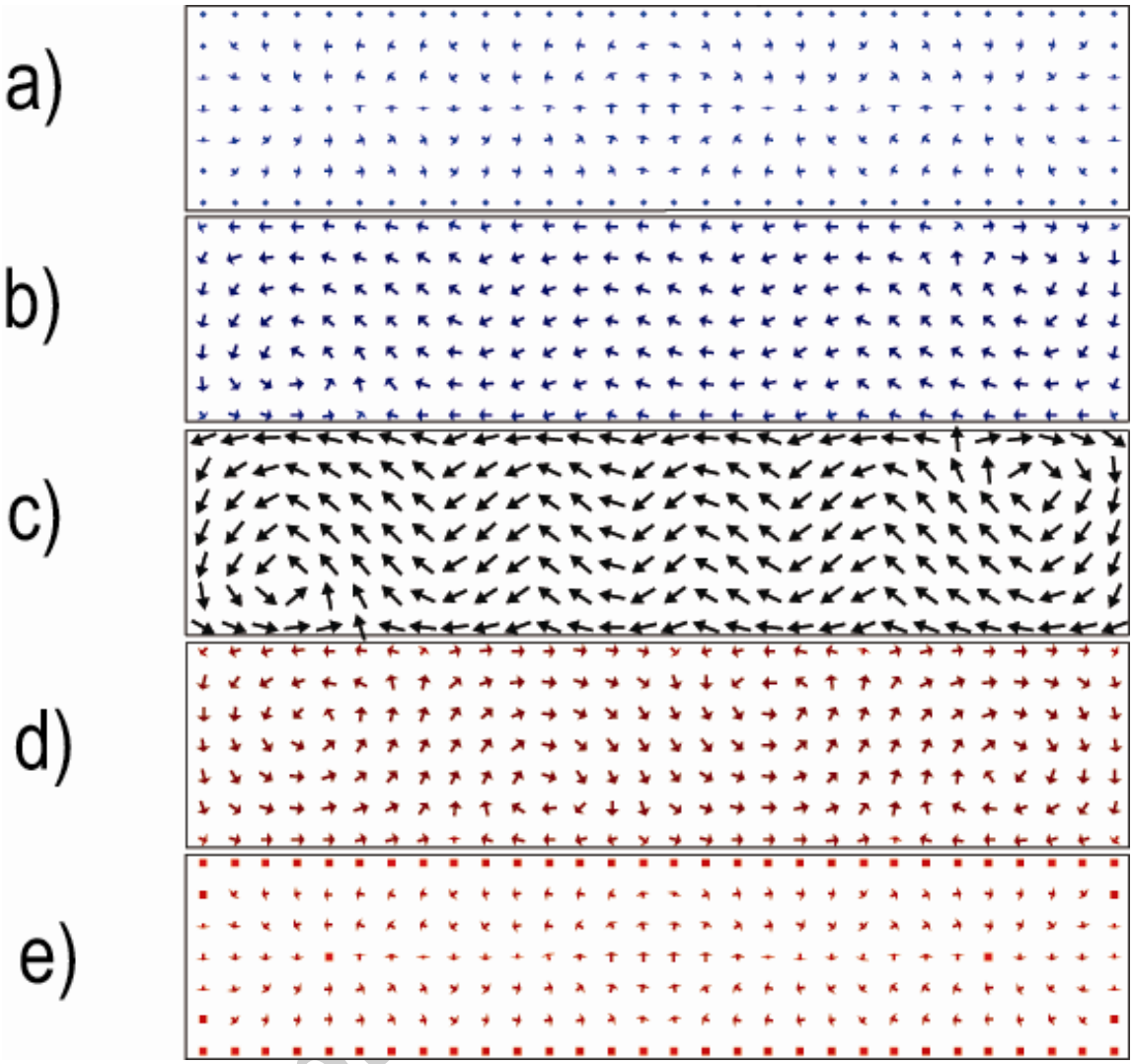

Fig. 4. Magnetization evolution in the microbelt plane as the magnetic field sweeping from positive high value to negative high value. The presented magnetic states are obtained at (a) high positive magnetic field, (b) intermediate positive field, (c) zero magnetic field, (d) negative intermediate field and (e) negative switching field.

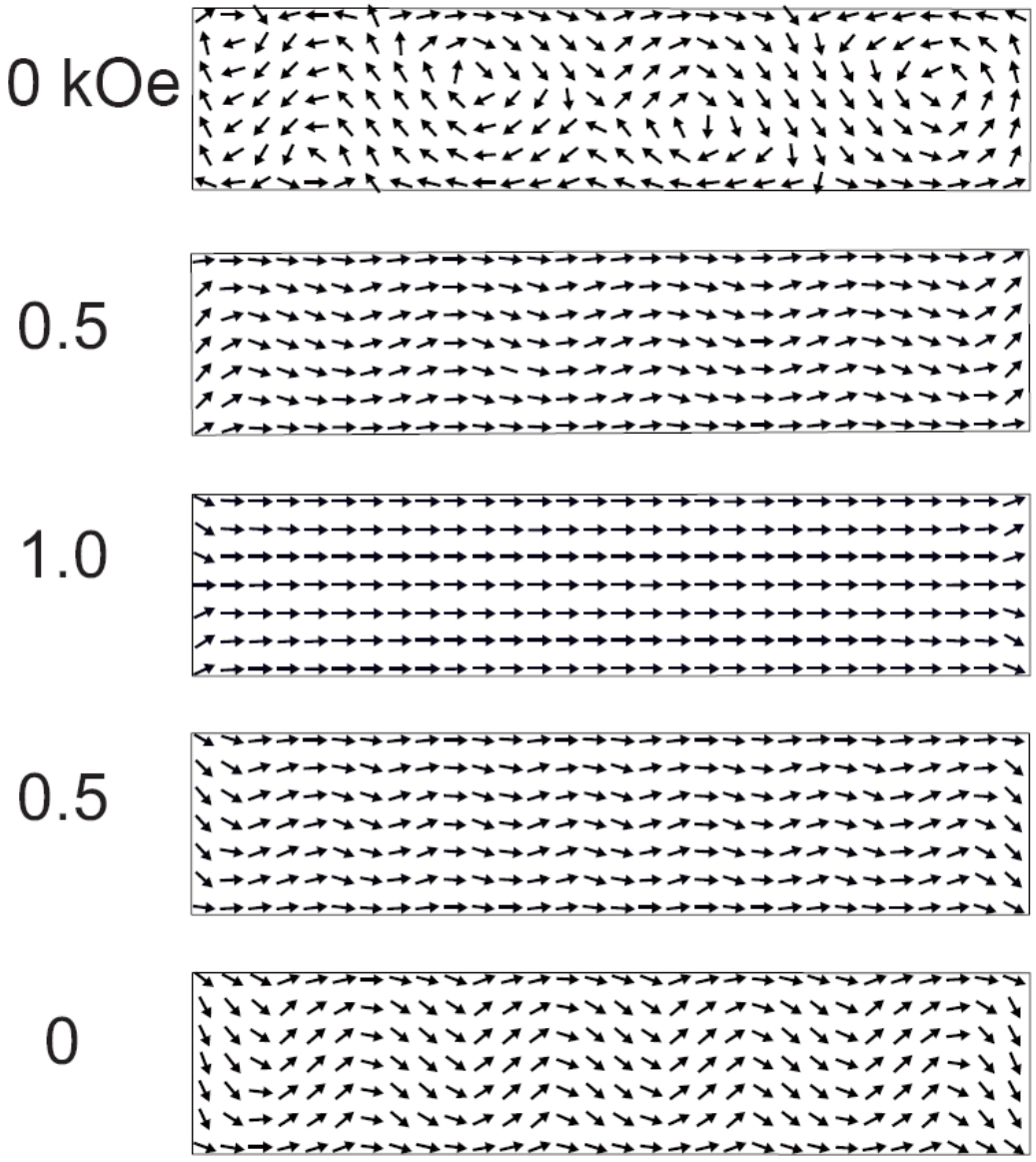

Fig. 5. Simulated magnetization configurations with the applied field as denoted with an incident angle of 15 degree.